The rice SCF^{OsFBK1} E3 ligase mediates jasmonic acid induced degradation of a RING-H2 protein and the cinnamoyl-CoA reductase, OsCCR14

Pratikshya Borah
University of Delhi - South Campus
Aishwarye Sharma
University of Delhi - South Campus
Jitendra Khurana (khuranaj@genomeindia.org)
University of Delhi - South Campus https://orcid.org/0000-0003-3808-1662

Research Article

Keywords: E3 ubiquitin ligase, jasmonate signalling, plant cell wall, plant hormone, protein degradation, protein stability, FLIM, confocal imaging

Posted Date: March 16th, 2021

DOI: https://doi.org/10.21203/rs.3.rs-300884/v1

Abstract

We had previously shown the rice F-box, OsFBK1, plays a role in anther development by mediating the turnover of OsCCR14, a cinnamoyl CoA-reductase regulating lignification. Another substrate identified in the same Y2H library screening was OsATL53, a member of the ATL family of RING-H2 proteins that is primarily localized to the cytoplasm. We found OsATL53 to be a component and substrate of SCF^{OsFBK1} by immunoprecipitation and cell-free studies. Incidentally, OsATL53 was found to interact with OsCCR14 in the cytoplasm and form a stable complex in cell-free experiments and bimolecular fluorescence complementation assays. Biochemically, OsATL53 was found to influence the enzymatic activity of OsCCR14 by decreasing its efficiency. Degradation studies have shown OsFBK1 mediates turnover of OsCCR14 in the nucleus, while OsATL53 is degraded in both cytoplasm and nucleus. The degradation of ATLs by F-box proteins has not been reported before. In presence of jasmonic acid (JA), which plays a role in anther dehiscence, OsATL53 has been found to gather around the nucleus, and this property enables the translocation of the OsATL53-OsCCR14 complex from a cytoplasmic localization to accumulate around the nuclear periphery. FLIM analyses revealed OsCCR14-OsATL53 complex undergoing conformational changes in presence of JA and this triggers OsFBK1 to mediate the targeted degradation of OsATL53 in the cytoplasm, thereby dissociating the cytoplasmic OsCCR14-OsATL53 complex and enabling OsCCR14 to enter the nucleus and eventually get degraded by SCF^{OsFBK1} E3 ligase. We have thus studied the signalling mechanism of a variant JA-induced E3 ligase-mediated substrate turnover in plants at the molecular level.

Introduction

Homeostasis in protein levels in all biological processes is a critical and essential regulatory mechanism. The onus of this regulation falls vastly on the ubiquitin 26S proteasome-mediated system (UPS) that is conserved across species. The ligases in the UPS participate in a range of concerted processes including substrate identification to mediating controlled ubiquitination of target proteins. The specificity in target protein recognition is particularly expanded in plants where there is a presence of an enormous number of E3 ligases as compared to animals (Jain *et al*., 2007, Hua *et al*., 2011). Plant E3 ligase genes vastly outnumber those of the other non-plant eukaryotes, where approximately 1400 E3 ligase encoding genes have been annotated in *Arabidopsis thaliana* genome and about 600 in the human genome (Vierstra, 2009, Buetow and Huang, 2016). Of the different classes of E3 ligases available, the RING-type family forms the largest group. The RING family of E3 ligases is characterized by the presence of the canonical RING domain that functions as an intermediary between E2-ubiquitin (Ub) and the E3 ligases. RING-based E3 ligases could be either single-subunit or multi-subunit. The cullin-RING E3 ligases (CRLs) are complex RING-type E3 ligases and amongst them the most abundant type found in plants is the SCF type (Vierstra, 2009, Hua and Vierstra, 2011).

The RING-finger domain found in RING-type E3 ligases is a specific type of zinc finger that binds two Zn ions in a ‘cross-brace’ structure using a defined pattern of cysteine (C) and histidine (H) residues found in its conserved aā sequence (Freemont, Hanson and Trowsdale, 1991). The C_3HC_4 (RING-HC) and $C_3H_2C_3$

(RING-H2) are the most common RING domains where RING-HC domain has been found in single polypeptide E3 ligases and RING-H2 domain is associated with complex multi-subunit E3 ligases (Jackson *et al.*, 2000). Apart from these domains, the presence of less frequent domains, like RING-v, RING-C2, RING-D, RING-S/T and RING-G type, has also been described (Jiménez-López *et al.*, 2018b). A staggering 551 potential E3 ligases have been reported in *Arabidopsis thaliana* where 451 correspond to RING-H2 variant and the proportion of this variant in species like *Brassica rapa* and *Oryza sativa* are 55% and 57%, respectively (Lim *et al.*, 2010; Alam *et al.*, 2017). It has been previously reported that some RING zinc finger protein genes are rapidly induced in response to elicitors and these genes are members of a family known as ATL (*Arabidopsis* Tóxicos en Levadura) (Salinas-Mondragón, Garcidueñas-Piña and Guzmán, 1999). These ATLs contain a variant RING-H2 in which the fifth cysteine residue has been substituted by a histidine residue. Mutants of ATLs have been previously isolated and analysed to reveal a link between these putative ubiquitin (Ub) ligases and plant defence signalling pathways (Serrano and Guzmán, 2004). It was also reported that the *Arabidopsis* family consisted of 80 members and rice had 121 ATL genes (Serrano *et al.*, 2006). In the past years, two new classes of RING E3 ligases have been identified in addition to ATLs, based on RING-H2 domain variations and RING-outside conserved motifs: BCA 2 Zinc-Finger (BZF) ATLs (BTLs) (Guzmán, 2014) and CTLs containing the YEELL conserved motif (Jiménez-López *et al.*, 2018a).

Several E3 RING-finger protein genes have been characterized over the years for their role in diverse processes; these include *CONSTITUTIVE PHOTOMORPHOGENIC 1 (COP1)* in light signalling (Deng *et al.*, 1992; Hardtke *et al.*, 2002), *SINA of Arabidopsis thaliana 5 (SINAT5)* in accentuating auxin signalling (Xie *et al.*, 2002; Xu and Li, 2003), *HIGH EXPRESSION OF OSMOTICALLY RESPONSIVE GENES 1 (HOS1)* in cold response (Dong *et al.*, 2006), *ACCUMULATION AND REPLICATION OF CHLOROPLASTS 1* in self-incompatibility (Stone *et al.*, 2003), *SHOOT APICAL MERISTEM ARREST 1* involved in shoot apical meristem maintenance (Sonoda *et al.*, 2007), *ABI1-INTERACTING PROTEIN 2* in ABA signalling (Zhang, Garreton and Chua, 2005), *RING-H2 GROUP F1A/RING-H2 GROUP F2A* in gametogenesis (Liu *et al.*, 2008) and *DEFECTIVE IN ANTHER DEHISCENCE 1 (DAD1)- ACTIVATING FACTOR (DAF)* that affects jasmonic acid (JA) biosynthesis (Peng *et al.*, 2013), to name a few. Several *ATL* genes that have been studied till date include *ARABIDOPSIS TÓXICOS EN LEVADURA 2 (ATL2)*, which participates in plant defence (Serrano and Guzmán, 2004), *ELICITOR 5 (EL5)* that regulates cell death during root development, and *DAY NEUTRAL FLOWERING (DFN)/AthATL62*, which participates in repressing photoperiod response (Guzmán, 2012). Some of the important CTLs characterized include *Arabidopsis* E3 ligase *BIG BROTHER (BB)* that regulates organ size (Disch *et al.*, 2006); the human *RNF11/ARKADIA* that is a TGF-signalling and DNA damage responsive SUMO E3 ligase coding gene (Poulsen *et al.*, 2013); *RNF 165/ARK2C* (Kelly *et al.*, 2013) and the p53 regulator *RNF38* (Sheren and Kassenbrock, 2013).

In the present study, we have investigated the rice ATL gene *OsATL53* that is a component of E3 ligase and interacts with OsCCR14 (OsCCR20 (Kawasaki *et al.*, 2006)), the substrate of the F-box protein, OsFBK1. These proteins, OsCCR14 and OsATL53, were identified as putative substrates of OsFBK1 in a Y2H screen using anther specific library, and the degradation of OsCCR14 by SCF^{OsFBK1} has been

described earlier that ultimately regulates lignification in rice anthers and roots (Borah and Khurana, 2018). We found that under the influence of JA, OsATL53 translocates the OsATL53-OsCCR14 complex from the cytosol towards the nucleus where these two substrates are degraded via OsFBK1 in different cellular compartments. Further, we have also shown that OsATL53 affects the enzymatic activity of OsCCR14. We have, therefore, tried to explore the degradation mechanism of protein factors (involved in anther development) in response to hormones like jasmonate, as well as provide a new insight into the function of RING-H2 ATL proteins.

Results

In our previous study (Borah and Khurana, 2018), we had identified a few putative substrates of SCF^{OsFBK1} E3 ligase by a Y2H anther library screening. The cinnamoyl-CoA reductase enzyme, OsCCR14 (previously designated as OsCCR20), involved in catalysing the second rate-limiting step in lignification, was found to be a substrate of SCF^{OsFBK1}; it was also shown to regulate rice anther lignification. The RING-H2 protein, OsATL53, was also identified as a putative substrate in the same library screening experiment. Our endeavour, therefore, was to investigate the role of OsATL53 with the aim to understand the molecular mechanism regulating its turnover and its possible relation to rice anther development. The physiological effects of such a mechanism are being currently investigated.

OsATL53 is a component of E3 ligase and interacts with both OsFBK1 and OsCCR14

OsATL53 (RING-H2 protein) is one of the 121 odd RING-H2 ATLs found in rice (Serrano *et al.*, 2006). The signature sequence of ATLs consists of residues that localise to the central region of the RING-H2 domain, viz. two cysteines corresponding to the third and sixth Zn ligands, two histidines occupying the fourth and fifth Zn ligands, a highly conserved proline amino acid that separates a residue upstream from the third Zn ligand and a highly conserved tryptophan that is placed three residues downstream from the sixth zinc ligand (Serrano *et al.*, 2006); this also holds true for OsATL53 (PxCxHxxHxxCxxxW, Fig. S1A). Sequence alignment between OsATL53 and known RBX1 proteins studied in humans, yeast and *Arabidopsis* has also shown that there is homology amongst these proteins (Fig. S1A), even though OsATL53 is not the direct homologue of the canonical RBX1 in reverse blast hits. ATL proteins are also known to comprise of an N-terminal region that is rich in hydrophobic amino acids, and the module generally comprises of a single hydrophobic region of at least 18 residues (Serrano *et al.*, 2006). OsATL53 also has been found to contain one N-terminal hydrophobic transmembrane domain of 22 amino acid residues (Fig. S1B).

In order to confirm whether OsATL53 could be a component of SCF E3 ligase, in vitro immunoprecipitation assay was carried out between GST-CUL5g ((Borah and Khurana, 2018) and 6xHis-OsATL53, and a weak interaction was detected in this assay (Fig. 1A). We had previously shown that the SCF^{OsFBK1} E3 ligase complex comprises of OSK1/20, CUL5g (non-standard nomenclature) and OsFBK1 employing Y2H assay (Borah and Khurana, 2018). Based on the above data obtained, it appears that the

complete SCF^{OsFBK1} complex also harbours OsATL53, probably as the RBX1 component (Fig. S1D), although it cannot be ruled out that OsATL53 can be a part of another RING-based E3 ligase.

A detailed study on the architecture of ATLs has suggested that there are two distinct regions in ATLs that are responsible for mediating protein-protein interactions; region I located at the amino-terminal end and region VII that is positioned towards the carboxy-terminal end (Aguilar-Hernández, Aguilar-Henonin and Guzmán, 2011). These two regions have been thought to be important in conferring the functional diversity to ATLs where they might be involved in either target recognition or in mediating the interaction with the components of the functional ubiquitin ligase (Aguilar-Hernández, Aguilar-Henonin and Guzmán, 2011). To test this hypothesis with our RING-H2 protein, we generated GST-tagged deletion constructs that had a truncated N-terminal, ΔOsATL53 (region I, including the transmembrane domain, amino acids from 1 to 32) and a truncated C-terminal end, OsATL53Δ (region VII, amino acids from 138 to 202), respectively (Fig. S1B for the graphical representation of the deletion constructs).

ATLs like DAF (DEFECTIVE IN ANTHER DEHISCENCE1-Activating Factor) have been previously described to have auto-ubiquitination activity (Peng *et al.*, 2013). First, we investigated the auto-ubiquitination activity of OsATL53 using a protocol described earlier (Peng *et al.*, 2013), with slight modifications. As is evident from Fig. 1B, OsATL53 has auto-ubiquitination activity and can probably function as an E3 ligase, while the truncated constructs functioning as negative controls showed little or no ubiquitination activity. ΔOsATL53 failed to display any auto-ubiquitination property, while OsATL53Δ showed diminished activity. These results also show that region I of OsATL53 is involved in ubiquitination activity. We also observed a slight shift in size without an apparent smear in the ubiquitinated form of OsATL53 (lane 4 of Fig. 1B) indicating that the addition of ubiquitin is probably in the mono form rather than poly-ubiquitination.

In general, RING-H2 proteins have been found to localise to different cellular compartments (Furukawa *et al.*, 2000; Greve *et al.*, 2003) and OsATL53 has been found to specifically localize to the cytoplasm of onion peel epidermal cells (Fig. 1C and Fig. S3). The red boxes around the nucleus of the target cell in the top (z-stacked cell) and middle (nuclear plane only) panel of Fig. 1C show the absence of EYFP fluorescence of OsATL53 in the nucleus while being abundant in the cytoplasm. For all our intracellular localisation experiments using confocal microscopy, we chose to work with onion epidermal cells as it is a monocot system, has a visibly distinguishable nucleus and is a standardized and widely used transient expression system in comparison to epidermal cells of *Nicotiana* (dicot), and rice protoplasts where the presence of a large vacuole may hamper the viewing of the localization dynamics. As stated earlier, OsATL53 was originally identified as one of the putative substrates of OsFBK1 in the Y2H anther library screening along with OsCCR14 (Borah and Khurana, 2018). This interaction was further confirmed by in vitro immunoprecipitation assay between GST-OsFBK1 and 6xHis-OsATL53 (Fig. 1D) and by split EYFP BiFC (Fig. 1E). However, the split EYFP interaction was found to be short-lived and required short incubation time after bombardment (10-12 h), indicating a labile interaction between the two proteins. While OsATL53 is localised solely to the cytoplasm, the split EYFP BiFC between OsFBK1 and OsATL53 showed a dominant cytoplasmic interaction along with a slight presence of the complex in the nucleus

(nuclear plane image, Fig. 1E); implying that the interaction between these proteins takes place in both cellular compartments, albeit with an overall cytoplasmic preference.

In a serendipitous experiment, OsATL53 was found to interact with OsCCR14 in a split EYFP BiFC experiment where the EYFP fluorescence was found scattered throughout the cytoplasm of the onion peel cells (Fig. 1E). This BiFC interaction was found to be stable even after 16 h post incubation after particle bombardment. This scattered appearance of fluorescence, however, did not match with any organellar localisation like that of mitochondria (data not shown). This interaction was further confirmed by in vitro immunoprecipitation (Fig. 1F). However, OsATL53 does not interact with OsCCR18 (OsCCR19 (Kawasaki *et al.*, 2006), Fig. S1E), the closest homologue of OsCCR14 described earlier (Borah and Khurana, 2018), indicating that the OsATL53-OsCCR14 interaction is specific.

In vitro immunoprecipitation assays were then carried out with OsFBK1 and OsCCR14 separately using both the deletion constructs: ΔOsATL53 and OsATL53Δ. As is evident from the western blot analyses, ΔOsATL53 interacts weakly with OsFBK1 while its interaction with OsCCR14 is unaffected, indicating that region I is involved in interacting with the components of the functional ubiquitin ligase. Whereas for OsATL53Δ, the interaction with OsCCR14 (or the target of SCF^{OsFBK1}) is vastly hampered, indicating that the C-terminal domain of OsATL53 is involved in target recognition as reported earlier (Aguilar-Hernández, Aguilar-Henonin and Guzmán, 2011). These experiments also strengthen the idea that RING-H2 proteins might have multiple roles apart from their property to function in the ubiquitination process *per se*. Putative models of OsATL53-OsCCR14 and OsFBK1-OsATL53-OsCCR14 interactions have also been generated by ab initio modelling (Fig. S2), to gain a perspective into the possible complex formation between these proteins. The models were checked by Ramachandran plot analyses.

OsATL53 is a substrate of OsFBK1 and is preferentially degraded in the cytoplasm

Since OsATL53 was identified as an interacting protein in the anther library Y2H screening using OsFBK1 as the bait (Borah and Khurana, 2018), we checked whether it is degraded by SCF^{OsFBK1}. By carrying out in vitro cell-free degradation assays using the total plant protein extracts of 7-day-old seedlings of wild-type (WT), vector control (VC) and *OsFBK1* transgenics, as described earlier (Borah and Khurana, 2018), it became evident that OsATL53 degradation is mediated by OsFBK1 *via* the 26S proteasome pathway (Fig. 2A and 2B).

We had earlier observed that the BiFC EYFP fluorescence showing interaction between OsFBK1-OsCCR14 was preferentially visible in the nuclei of onion peel cells, with weak signals detectable in the cytoplasm (Fig. 2C; see also (Borah and Khurana, 2018)), while that of OsFBK1-OsATL53 was detected preferentially in the cytoplasm with a weak signal visible in the nucleus (Fig. 1E and 2E). Such interactions in specific cellular compartments could provide hint at the target proteins' sites of degradation mediated by SCF^{OsFBK1} E3 ligase. To prove our assumption, we carried out separate cell-free degradation assays of 6xHis-OsCCR14 and 6xHis-OsATL53 in both nuclear and cytoplasmic protein extracts of $OsFBK1^{OE}$ and WT lines. The data presented in Fig. 2C and 2D show that degradation of OsCCR14 takes place

specifically in the presence of nuclear protein-enriched extracts under the given experimental duration; while Fig. 2E and 2F show that OsATL53 is degraded in both the protein fractions; it is degraded preferentially in the cytoplasmic protein fraction in comparison to the nuclear protein-enriched extracts within the same assay duration. Curiously, the degradation kinetics for both OsCCR14 and OsATL53 in the respective dominant enriched protein fractions is marginally faster than that observed for total plant protein extracts in the same experimental duration. These experiments provide evidence that OsCCR14, as a substrate of SCF^{OsFBK1}, is degraded preferentially in the nuclear protein extracts; while OsATL53 is degraded by SCF^{OsFBK1} in both the nuclear protein-enriched and cytoplasmic protein fractions, with a preference for the cytoplasmic protein extracts. Hence, the BiFC fluorescence signals observed for both OsCCR14 and OsATL53 with OsFBK1 indeed indicate the sites of interaction where their subsequent degradation takes place. The labile split-EYFP signals observed for OsFBK1-OsATL53 interaction (Fig. 1E) also correspond to the faster degradation kinetics of OsATL53 mediated by SCF^{OsFBK1}. That cytosolic enzymes like OsCCR14 are degraded specifically in the nucleus and mediated by F-box proteins find support from some earlier studies in animal systems (D'Angiolella *et al.*, 2012).

Jasmonic acid changes the dynamics of the OsCCR14-OsATL53 complex

The process of anther dehiscence preceding pollination is characterised by three distinct events: lignification of the secondary walls in endothecial cells, degradation of the septum cells to form a bi-locular anther, and the release of pollen grains by the breakage of the septum (Goldberg, Beals and Sanders, 1993). In this process of anthesis, auxin has been shown to regulate the commencement of anther dehiscence by controlling the timing of the lignification process at the start of late stamen development (Cecchetti *et al.*, 2008). Various studies have shown that jasmonic acid (JA) is also involved in the control of anther dehiscence mainly in the late stamen development stages (Xie *et al.*, 1998; Stintzi and Browse, 2000; Ishiguro *et al.*, 2001; Devoto *et al.*, 2002). JA is thought to initiate anther dehydration by controlling the transport of water in the anther filament, which in turn triggers stomium breakage and opening at the final stages of anther development (Sanders *et al.*, 2000; Ishiguro *et al.*, 2001). Thus, it has been suggested that an auxin maximum at early floral stages in *Arabidopsis* blocks premature endothecium lignification, and its decline in the later stages triggers endothecium lignification. This reduction in the auxin concentration also leads to the increase in JA concentration, thereby causing stomium breakage and anther dehiscence (Cecchetti *et al.*, 2013).

We had previously shown that process of degradation of OsCCR14 (the enzyme catalysing the second rate-limiting step in lignin formation) by SCF^{OsFBK1} is not affected by auxin, but transcription of *OsCCR14* is induced by auxin (Borah and Khurana, 2018). However, keeping in mind that JA affects the process of anthesis, JA might regulate the process of OsCCR14 degradation to affect anther lignification. Based on this assumption, we first carried out particle bombardment on onion peel epidermal cells of the various constructs (Fig. S3) and treated the peels with 6.4 mM JA for 4 h to check whether JA affects the localization dynamics of these proteins (Fig. S3). The concentration of JA used in our assay (6.4 mM) was as deployed in an earlier study (Cecchetti *et al.*, 2013) that triggered precocious anthesis in

Arabidopsis faster than that observed earlier (Stintzi and Browse, 2000). Since 6.4 mM JA is considerably higher than normal physiological conditions, we first tested the effect of this concentration of JA in onion epidermal cells bombarded by various constructs. We found that the localization patterns of OsFBK1, OsCCR14 and the vector controls were found to be unaffected by JA, even after 4 h of incubation. F-boxes are known to function as hormone receptors (*3*), but since the localization of OsFBK1 was unaffected after the application of JA to the bombarded cells (Fig. S3), we can presume that OsFBK1 does not function as a JA sensor. However, the EYFP fluorescence of OsATL53 appeared to accumulate around the nucleus but did not enter the nucleus (Fig. S3 and Fig. S4; for cells with nuclear stain). This accumulation of OsATL53 around the nucleus was seen to initiate as early as 2 h post incubation (data not shown). In order to rule out the effect of stress caused by a high JA concentration in the bombarded cells during the experimental time frame, we checked the changes in lifetime of EYFP-OsATL53 on exposure to a 6.4 mM JA by FLIM confocal microscopy (Fig. S5B), as the lifetimes of fluorophores are affected by the cellular pH and ionic changes amongst other factors (Trautmann *et al.*, 2013). Even after 4 h of incubation with 6.4 mM JA, the lifetime of EYFP-OsATL53 did not change (Fig. S5C). A representative stressed or plasmolysed cell expressing EYFP-OsATL53 is also shown as a control that displays a decrease in lifetime due to changes in cell integrity (Fig. S5B and S5C). Further, we also checked the changes in localization of EYFP-OsATL53 with 100 µM JA, the concentration used in experiments done earlier (Stintzi and Browse, 2000). However, changes in localization of EYFP-OsATL53 were observed to initiate only after 8 h of incubation with 100 µM JA as opposed to 2 h when 6.4 mM JA was used (Fig. S4A). Due to the large difference in the time of incubation and the reason that both concentrations do not affect the cellular integrity, we chose to use 6.4 mM JA for all further experiments.

We had also observed that OsATL53 and OsCCR14 interacted with each other, therefore, we carried out co-localization studies using respective constructs and subjected the bombarded onion peel cells to JA treatment for 4 h. As is evident from Fig. 3A, a distinct accumulation of EYFP (OsATL53) and ECFP (OsCCR14) fluorescence is observed around the nucleus after 4 h of JA treatment. While the localization of OsCCR14 is unaffected by JA when present alone (Fig. S3), there is a definite presence of OsCCR14 fluorescence along with OsATL53 around the nucleus after JA treatment. This implies that the localization of the complex of OsCCR14-OsATL53 is affected by JA, presumably mediated by the movement of OsATL53 towards the nucleus on exposure to JA (Fig. 3A). On the other hand, co-localization of OsFBK1-OsATL53 and OsFBK1-OsCCR14, respectively, were unaffected even in the presence of JA (Fig. S6). However, in both the absence and presence of JA, OsATL53 was found to be present slightly in the nucleus when co-localized with OsFBK1 (Fig. S6). This observation for OsCCR14-OsATL53 complex localization in response to/without JA was also repeated using BiFC interaction studies (Fig. 3B, OsCCR14-nEYFPC_1 and OsATL53-cEYFPN_1). However, we failed to observe any EYFP fluorescence of the BiFC interaction beyond 4 h of JA exposure.

Additionally, we also investigated whether, apart from the movement of the OsCCR14-OsATL53 complex and its accumulation around the nuclear periphery, JA also induces structural changes in this complex. For this we adopted the FLIM-FRET (Fluorescence Lifetime Imaging- FÖrster Resonance Energy Transfer)

technique to examine any changes in the lifetime of the ECFP-donor construct with/without JA. This technique of FLIM-FRET using the latest Leica SP8 Falcon confocal microscope has been recently used to study the essential role played by the Zn+ transporter ZIP7 in B cell development in mice (Anzilotti *et al.*, 2019). Since we already know by BiFC analysis that OsCCR14 and OsATL53 interact in a particular vector combination that allows the split EYFP to come close together for fluorescence, thus, we used FRET probes that have both the fluorescent probes (ECFP and EYFP) in the N-terminal regions, and technically will be separated beyond the required FÖrster distance (<10 nm). As expected, the lifetime of the donor ECFP (~3 ns in solution, https://www.fpbase.org/,(Lambert, 2019)) did not change under FLIM-FRET condition (Fig. 3C and 3D). However, when we added JA and incubated the bombarded onion peel cells for 2 hours, we noticed that the lifetime of the donor ECFP had decreased in FLIM-FRET conditions indicating a positive FRET (Fig. 3C and 3D). Positive FRET was not only observed around the nucleus where the ECFP-OsCCR14 and EYFP-OsATL53 fluorescence were found to accumulate, but also throughout the cell (Fig. 3D). *This meant that the addition of JA induces a certain conformational change to the OsCCR14-OsATL53 complex that enables the two FRET probes to come within the minimum FÖrster distance and cause energy transfer.* Such a change in donor lifetime was not observed in the control (OsFBK1-EGFP donor, EYFP-OsCCR14 acceptor) (Fig. S7). Such conformational changes might also explain the reasons behind the non-observation of BiFC EYFP fluorescence between OsCCR14-OsATL53 after 4 h of JA exposure (Fig. 3).

We had also mentioned that the BiFC interaction between OsCCR14-OsATL53 was stable for long duration post incubation after particle bombardment. However, JA affected the localization of the split-EYFP interaction between these two proteins in the onion epidermal peel cells. Therefore, we wanted to investigate whether JA plays a role in maintaining the stability of the OsCCR14-OsATL53 complex in rice. To explore this possibility, we carried out cell-free degradation using bacterially expressed 6xHis-OsCCR14 and 6xHis-OsATL53 purified protein fractions and incubating them with the whole protein extracts of WT rice seedlings as described previously (Borah and Khurana, 2018). It is clear from Figure 3C that JA affects the stability of OsCCR14-OsATL53 complex after 4 h of treatment by hastening the degradation of OsATL53, without affecting the stability of OsCCR14 during the experimental timeframe. However, in the absence of JA, OsATL53 has been found to be stable in the cell-free experiments when present as a complex with OsCCR14 (Fig. 3E). This is a stark contrast to the observation where the half-life of OsATL53 has been found to be considerably less when present alone in the cell-free experiments (Fig. 2A). The results of the cell-free experiments have been quantified and graphically represented in Fig. 3F. *These observations lead us to speculate that OsATL53 might interact with OsCCR14 to form a complex and probably attenuates the enzymatic reactions carried out by OsCCR14 in the lignification process and is turned over by* SCF^{OsFBK1} *when present alone.*

Jasmonic acid induces changes in the OsFBK1/OsCCR14-OsATL53 interaction and localization dynamics

It is apparent from the data presented above that OsFBK1 interacts with both OsCCR14 and OsATL53 individually to mediate their degradation via the 26S proteasome pathway in different cellular

components. We had also observed that OsATL53 probably enters the nucleus while forming a complex with OsFBK1 (Fig. 1E and Fig. S6). Keeping in mind these observations, it was imperative to check the nature of interaction between OsFBK1 and OsCCR14-OsATL53 complex and determine whether JA affects interaction amongst all these proteins. For this, we carried out particle bombardment for a three-way interaction amongst ECFP-OsFBK1 and OsCCR14-OsATL53 split EYFP. The upper panel in Fig. 4 shows that under normal untreated conditions, OsFBK1 does not seem to overly interact with OsCCR14-OsATL53 complex and follows its normal localization pattern, although some minor interactions could also be seen (Fig. 4A, upper panel). However, when the bombarded onion epidermal peels were treated with JA (+MG132) and incubated for 4 h, a drastic change in the dynamics of the interactions amongst the three proteins was observed (lower panel, Fig. 4A). The green colour shows the overlapping regions between the ECFP and EYFP fluorescence and it also shows that OsFBK1 interacted with OsCCR14-OsATL53 complex while accumulating around the nucleus, as observed earlier for JA treated OsCCR14-OsATL53 EYFP fluorescence. At the same time, in most cells we could also see that OsFBK1 has migrated out of the nucleus into the cytoplasm to interact with the OsCCR14-OsATL53 complex (Fig. 4A and B). Curiously, we did not observe any such behaviour for OsFBK1 alone when treated with JA (Fig. S3). Further, we also observed that on exposure to JA alone (-MG132), there was a loss of EYFP signal in the target cells indicating the disruption of the OsCCR14-OsATL53 complex and the possible degradation of the components in the respective compartments, as also proved by the cell-free studies (Fig. 4B, Fig. S8). At the same time, the localization pattern of OsFBK1 also seemed to change back to its original state after this process of degradation is over and its fluorescence appeared throughout the cell and in the nucleus (Fig. 4B). We had also noticed that some target cells exhibited faster movement and degradation kinetics, some initiating as sooner as 40 min post JA treatment (Fig. 4B) in the absence of MG132 as compared to the cell-free studies (Fig. 3E and F). This is expected as the cell-free studies had considerably higher substrate concentration (5 µg) than available in native cellular conditions.

OsATL53 attenuates enzymatic activity of OsCCR14

Finally, since OsATL53 forms a stable complex with OsCCR14 in the cytoplasm, we investigated whether it affects the enzymatic activity of OsCCR14. OsCCR14 is a cytosolic enzyme and has been found to preferentially reduce feruloyl-CoA esters into coniferaldehyde in the cytoplasm (Park *et al.*, 2017). Similarly, SbCCR1 (the sorghum ortholog of OsCCR14) also has a higher affinity for feruloyl-CoA ester as a substrate as opposed to the other esters (p-coumaroyl CoA, sinapoyl-CoA) (Sattler *et al.*, 2017). Thus, we chose feruloyl-CoA as a substrate for investigating the enzymatic activity of OsCCR14 alone, and in complex with OsATL53 (with/without JA). Feruloyl-CoA ester was prepared following the protocol described earlier (Park *et al.*, 2017; Sattler *et al.*, 2017) and used as substrate for the reaction mix comprising of: a) OsCCR14, b) OsCCR14 + OsATL53, c) OsATL53, d) OsCCR14 + OsATL53 + JA, and e) OsCCR14 + JA.

As evident from Fig. 5A, OsCCR14 shows a K_m of 6 µM, whereas the formation of a complex with OsATL53 demonstrates a significant reduction in the substrate affinity of OsCCR14 (K_m 20 µM). The addition of JA to either OsCCR14 or to the complex, however, does not affect the K_m values of OsCCR14

and the OsCCR14-OsATL53 complex, respectively, but slightly affects both their K_{cat} values (Fig. 5B), thereby signifying a marginal decrease in enzyme activity.

Our data clearly show that OsATL53 attenuates the enzymatic activity of OsCCR14 by significantly reducing its affinity for its desired substrate, feruloyl-CoA, without totally inhibiting its enzymatic activity. We might speculate at this juncture that OsATL53 acts as an allosteric effector molecule rather than an inhibitor. However, it would require detailed biochemical experimentation to confirm this assumption. Additionally, the presence of JA does not reduce the substrate affinity of OsCCR14 as a complex with OsATL53 any further, but the changes brought about in the conformation of the complex in its presence (as shown earlier, Fig. 3) is a trigger for the translocation of the complex towards the nucleus, and for OsFBK1 to recognise the complex as a substrate to initiate its degradation via the 26S proteasome pathway (Fig. 4).

However, based on our data in its current form, we cannot comment whether the ternary complex of OsFBK1-OsATL53-OsCCR14 enters the nucleus as a unit or whether they enter as separate binary complexes after partial degradation of OsATL53. We intend to pursue the molecular and biochemical factors involved in this JA induced changes in the OsFBK1/OsCCR14-OsATL53 interaction and localization dynamics. Additionally, the effects of such interaction between OsATL53 and OsCCR14 at the physiological level is currently being worked upon by the generation of knock-down rice transgenics. Our data also strongly indicate that there might be other protein partners at play or the presence of a unique signalling mechanism that remains elusive presently.

Discussion

The ATL family of RING-H2 proteins are a dynamic group that has been studied in the recent years. Several ATL proteins have been explored in *Arabidopsis* and other plant species and diverse functions have been attributed to them (Guzmán, 2012). The *Arabidopsis* and rice ATL family of RING-H2 proteins have been phylogenetically distributed into several clades based on their architecture and this large family of proteins are thought to be functioning as putative ubiquitin ligases of the RING-H2 type (Serrano *et al.*, 2006). The diversity in the architecture of the ATLs has been proposed to recognise and target substrates in different cellular environments (Aguilar-Hernández, Aguilar-Henonin and Guzmán, 2011). The ATL in our study was previously identified as OsATL53 and assigned to clade ‘k’ and is one of the few ATLs that is encoded by a gene containing introns (Serrano *et al.*, 2006). We found OsATL53 to be a component of a putative SCF^{OsFBK1} and to have auto-ubiquitination properties (Fig. 1). Based on the results obtained by our previous Y2H anther library screening experiments (Borah and Khurana, 2018), we confirmed that OsATL53 interacts with the F-box protein OsFBK1 and also with the cinnamoyl CoA-reductase enzyme OsCCR14, which was also a substrate of OsFBK1 (Fig. 1). However, the cellular localization of these two interactions differed indicating that OsATL53 interacts with these two proteins differently. These variations in the interactions could be due to the different domains present in OsATL53 as described earlier (Aguilar-Hernández, Aguilar-Henonin and Guzmán, 2011) and have been proved true by deletion studies (Fig. 1).

We found that OsFBK1 degrades OsATL53 and this degradation is pronounced in the cytoplasmic extract as compared to nuclear extract, which is in stark contrast to the degradation dynamics of OsCCR14 (Fig. 2). Seeing that both these proteins are substrates of SCF^{OsFBK1} and, OsATL53 itself is likely to be a component of the same E3 ligase, it appears that OsATL53 performs other functions apart from participating in the ubiquitination process. However, RING-H2 or ATLs being recognised as substrates by F-box proteins and degraded by them have not reported before. OsCCR14 has been found to be the closest homologue to AtCCR1 and has been suggested to be primarily involved in actively lignifying tissues like stems and roots (Park *et al.*, 2017). It was also found that OsCCR14 expresses constitutively throughout the various developmental stages of rice (Park *et al.*, 2017). Since OsCCR14 and OsATL53 were both identified as single target clones in the anther library, we speculate that these two proteins might be together involved in the lignification process and, from the rice anther development point-of-view, OsATL53 might also be involved in the degradation process of OsCCR14 after anther lignification process is over. Jasmonic acid has been previously studied extensively for its role in anther dehiscence (Sanders *et al.*, 2000; Ishiguro *et al.*, 2001; Cecchetti *et al.*, 2013). Additionally, the ubiquitin system and jasmonate signalling pathway are closely linked where the ubiquitin system contributes to the regulation of the synthesis, perception and signal transduction of JA (Nagels Durand, Pauwels and Goossens, 2016). Keeping these facts in mind, we investigated the effect of JA on the interactions between OsATL53-OsFBK1 and OsCCR14-OsATL53. While the interaction between OsATL53-OsFBK1 was unaffected by JA, OsCCR14-OsATL53 complex was found to accumulate around the nucleus when treated with JA (Fig. 3). This movement towards the nucleus after JA treatment has been observed for OsATL53 alone also (Fig. S3), and thus the accumulation of the OsCCR14-OsATL53 complex around the nucleus could be attributed to OsATL53.

Although, OsCCR14 can enter the nucleus on its own, it is not capable of transporting OsATL53 into the nucleus (Fig. 3). However, this is not the case for the OsFBK1-OsATL53 complex where OsATL53 seems to have entered the nucleus with the ‘assistance’ of OsFBK1 (Fig. S6) and this process seems to be unaffected by JA. We had seen that under the influence of JA, the erstwhile stable OsCCR14-OsATL53 complex was translocated around the nucleus, and that OsATL53 is degraded both in the cytoplasm and the nucleus and OsCCR14 is degraded solely in the nucleus. We had also seen that JA induces conformational changes in the OsCCR14-OsATL53 complex (Fig. 3C-D, Fig. S7). Based on these observations, we assumed that JA somehow disrupts the stability of the OsCCR14-OsATL53 complex, thereby enabling the targeted destruction of both the components by SCF^{OsFBK1} in their respective cellular compartments. Fig. 4B and Fig. S8 clearly show that JA indeed destabilises the OsCCR14-OsATL53 complex in the cytoplasm and results in the rapid degradation of OsATL53. This was further shown in the cell-free studies too (Fig. 2). Incredibly, OsATL53 was found to be stable as a complex with OsCCR14 in the absence of JA. RBX1 RING-H2 proteins have been quoted to “function as allosteric activators of E2 enzymes and play an essential role in ubiquitination process, although their precise mechanism of action is unknown” (Freemont, 2000; Jackson *et al.*, 2000; Noureddine *et al.*, 2002), which made us wonder whether plant ATLs might also participate in other enzymatic processes apart from ubiquitination of

target substrates. Thus, we provide evidence that the RING-H2/ATL protein, OsATL53, interacts with OsCCR14 and might function to decrease its enzymatic activity.

Further, we still needed to account for the role of OsFBK1 in this JA-induced translocation of OsCCR14-OsATL53 complex. We found that in an uninduced state, OsFBK1 does not interact with the OsCCR14-OsATL53 complex even though it interacts with the proteins individually (Fig. 4A). But, as soon as JA is applied, we see a change in the localization of OsFBK1 in the cell, whereby OsFBK1 not only interacts with the OsCCR14-OsATL53 complex in the cytoplasm but also travels with the complex towards the nucleus (albeit not appearing to enter the nucleus with the OsCCR14-OsATL53 complex) (Fig. 4A). At the same time, we had also shown that OsFBK1 mediates the degradation of OsATL53 in the cytoplasm (Fig. 2E and 3E). Based on these data, we believe that during this time, after JA exposure, OsFBK1 starts to mediate the degradation of OsATL53 in the cytoplasm, thereby destabilising the OsCCR14-OsATL53 complex and enabling OsCCR14 and the remaining OsATL53 to enter the nucleus to be degraded via the 26S proteasome and mediated by SCF^{OsFBK1}. We also believe that the JA-induced conformational changes brought about in the OsCCR14-OsATL53 complex (Fig. 3C and D) might be the trigger for the movement and subsequent degradation of the complex by OsFBK1, even though we are not aware of the factors involved in such a phenomenon at the molecular level at present. Such conformational changes brought about by JA in proteins and their subsequent degradation by the 26S proteasome have been previously reported for the JAZ degron (Sheard *et al.*, 2010).

From the biological point-of-view and to determine whether OsATL53 has a role in regulating the functions of OsCCR14, we examined the dynamics of enzymatic activities of OsCCR14 both alone and as a complex with OsATL53, in the presence and absence of JA, respectively. Since OsCCR14 catalyses the first limiting step in lignin formation in the cell cytoplasm, our data reveals that OsATL53 slows down the enzymatic processes of OsCCR14 and, thereby, functions to regulate lignification. Microarray data obtained from previously conducted experiments (Jain *et al.*, 2007) have shown that the expressions of *OsCCR14* and *OsATL53* overlap in tissues like roots of 7-day-old seedlings, inflorescence stages like P4 and P6 and seed stage S5, whereas their expression differs in the other stages of development examined (Fig. S8). Based on these data, it can be suggested that OsATL53 affects the lignification processes catalysed by OsCCR14 in different target tissues depending on the requirements of that development stage of rice plant. The presence of JA in tissues like late anther stages, however, changes the dynamics of the enzymatic processes and signals the recognition of the OsATL53-OsCCR14 as substrates for destruction via the SCF^{OsFBK1} E3 ligase.

Finally, to explain all the evidences we generated coherently in context to rice anther development (as both OsCCR14 and OsATL53 were screened in yeast anther library), we propose the following model (Fig. 6): During the initial anther development stages where lignification is controlled by auxin, OsCCR14 executes its enzymatic processes in the cytoplasm whereas the increased presence of OsATL53 in the later stages reduces this enzymatic activity. However, towards the later stages of anther maturation preceding dehiscence, when the level of JA starts to increase, the process of lignification needs to cease, and the proteins involved need to be turned over. At this stage, the presence of increasing levels of JA in

the cell might change the conformation of the OsCCR14-OsATL53 complex thereby triggering OsATL53 to travel towards the nucleus (via as yet unknown mechanism), while carrying OsCCR14 along with it as a payload. Although OsFBK1 previously did not interact with the complex but this JA-induced movement of the OsCCR14-OsATL53 complex towards the nucleus as substrates is recognised by OsFBK1 (mechanism remains unknown). At the same time, the substrate(s) bound functional SCF^{OsFBK1} E3 ligase might initiate the degradation of OsATL53, thereby disassociating the OsCCR14-OsATL53 complex. This would in turn enable OsCCR14 to enter the nucleus where it is degraded by the 26S proteasome. Also, some of the remaining OsATL53 might enter the nucleus as an OsFBK1-OsATL53 complex where OsATL53 would also be finally degraded via the nuclear 26S proteasome, mediated by the SCF^{OsFBK1} E3 ligase.

To summarise, we have reported a divergent role of ATL RING-H2 proteins in interacting with other proteins, regulating their activities, and in turn become substrates of E3 ligases, thereby highlighting the diversity in their functions apart from participating as a bridging partner between the E3 and E2 ligases. Additionally, the modulation of OsCCR14 enzymatic function by OsATL53 could have application in terms of manipulating the lignin content in cash crops. At the same time, we could also gain an insight into the functioning of the F-box protein, OsFBK1, in targeted substrate degradation that would in turn regulate anther development in rice with precision. We have also tried to highlight a possible pathway of substrate degradation that is triggered by jasmonate.

Methods

Gene constructs

The 609 bp of the *OsATL53* gene (LOC_Os04g48310) was cloned in the following vectors: pET28a (*Eco*RI/*Sac*I) (Novagen); pGEX4T1 (*Eco*RI/*Sal*I) (GE); pENTR-D-TOPO (5′ CACC overhang) entry vector and BiFC Gateway™ vectors, pSITE-3CA-EYFPC_1 and pSITE-3CA-EYFPN_1 using Gateway™ technology (pENTR™ Directional TOPO® cloning kit, and LR clonase Enzyme mix II kit; Invitrogen Inc. USA). *CUL5g* (LOC_Os05g05700) was cloned in pGEX4T1 vector (*Bam*HI/*Sal*I). The deleted constructs of *OsATL53* (510 bp of *ΔOsATL53*, 411 bp of *OsATL53Δ*) were cloned in the pGEX4T1 vector (*Eco*RI/*Xho*I). The cloning of *OsFBK1* (LOC_Os01g47050) and *OsCCR14* (LOC_Os08g34280), in their respective vectors has been described earlier (Borah and Khurana, 2018). For localization and FLIM-FRET experiments, pSITE-1CA/pCAMBIA1302 was used for the donor constructs and pSITE-3CA for the acceptor constructs. Additionally, OsFBK1 was cloned in the pSITE-1CA vector for CFP fluorescence by Gateway™ cloning. The amplification of the genes was carried out using Phusion™ high-fidelity Taq polymerase (Finnzymes, Finland) as per manufacturer's instructions (see Supplemental Table S1 for primers).

Particle bombardment

Biolistics of the various constructs on onion epidermal peel cells for BiFC, intercellular localization and hormone assays were carried out using Biolistic PDS-1000/He particle delivery system (Bio-Rad, USA) as described earlier (Borah and Khurana, 2018). For hormone-related visualisation, the bombarded and

incubated onion peels (12-16 h) were treated with 6.4 mM JA for the requisite time-points before observing for fluorescence under confocal microscope (Leica TCS, SP5). For FLIM-FRET experiments, all observations and analyses were carried out using the Leica SP8 FALCON confocal microscope at the Central Instrumentation Facility (CIF), University of Delhi South Campus. FLIM was carried out at 40 MHz and curve-fitting was carried out using the n-Exponential Reconvolution fit model. For all experiments, the tissue was mounted in water and observed at 20X magnification. All experiments were carried out at least five times, with an average of 3 cells being visualised in each repetition.

Protein induction, western blotting and immunoprecipitation

Induction and western blotting of 6xHis-OsATL53, 6xHis-OsCCR14, GST-OsATL53, GST-OsFBK1 and GST-Cul5g was carried out as described earlier (Borah and Khurana, 2018). Immunoprecipitation assays were performed using 100 µg of unpurified bait and prey protein lysates as per the protocol described earlier (Borah and Khurana, 2018). Pre-stained markers used for all blots were Puregene NEX-GEN-PinkADD pre-stained protein ladder (Cat. # PG500-0500PI, Genetix Asia Pvt. Ltd., New Delhi, India). Western blotting was carried out with anti-His (Cat. # H1029-5ML, Sigma, USA) and anti-GST (Cat. # G7781-2ML, Sigma, USA) antibodies.

Auto-ubiquitination assay

The auto-ubiquitination activity of OsATL53 was carried out following the protocol described by Peng et al. (2013) with slight modifications. An E1 and E2 ligase mix (Cat. # U8382, Sigma, USA) was used for the activation and conjugation of ubiquitin. Negative controls used were generated in the laboratory. Probing of ubiquitin was done using monoclonal anti-ubiquitin antibodies (Cat. # U0508-50UL, Sigma, USA) at a dilution of 1:8,000+1% BSA.

Cell-free degradation

For cell-free degradation assays, total plant protein was extracted from 7-day-old seedlings of WT and OsFBK1 transgenics and cell-free experiments were carried out using 5 µg 6xHis-OsATL53/5 µg 6xHis-OsCCR14 in 30 µg total plant protein extracts/nuclear-enriched protein extracts/cytoplasmic protein extracts by following the protocol described before (Borah and Khurana, 2018). Nuclear protein extracts from 10-day-old seedlings (5 g tissue) were obtained as per protocol described by (Xu et al., 2012). The cytoplasmic extracts were aliquoted after filtration and the first centrifugation step. For loading controls, the same blots were stained with Ponceau for the detection of the Rubisco protein large subunit band for cell-free with total plant protein and cytoplasmic extracts whereas for cell-free with the nuclear-enriched protein extracts, Ponceau stained histone H3 band (~15kDa) was used as loading control. For cell-free experiments with JA, the cell-free degradation cocktail was mixed with 6.4 mM JA and incubated at 30 ^{o}C for the requisite time points. The degradation data was graphically represented by measuring the intensities of the bands of all blots in Image Studio^{TM} Lite ver. 5.2 (https://www.licor.com/bio/products/software/image_studio_lite/). The 2 h/6 h western band for each blot of OsATL53 and OsCCR14, respectively, was used as the reference and measured intensities were

normalised against it and multiplied by 100. Representation of the data is in percentage intensity ratio. All experiments were carried out at least thrice and error bars denote standard deviation across replicates.

Synthesis of feruloyl-CoA thioester and purification

The protocol for synthesis of the substrate feruloyl-CoA thioester was modified from the processes described earlier (Park *et al.*, 2017; Sattler *et al.*, 2017). Briefly, the *Arabidopsis4-coumarate: CoA ligase 1* gene, *At4CL1*, was amplified from leaf cDNA and cloned in pET28a vector (see Table S1 for primers). The clone was transformed in BL21-RIL competent cells and the protein induced and purified as described earlier (Borah and Khurana, 2018). For the synthesis of the thioester, 410 µg of purified At4CL1 protein was added to a 40 mL solution containing 50 mM sodium phosphate buffer, pH 7.0, 800 µM CoA (Cat. # C4282, Sigma, USA), 2.5 mM ATP (Cat. # A-7699, Sigma, USA), 2 mM ferulic acid (Cat. # 128708, Sigma, USA) and 5 mM $MgCl_2$. The reaction mix was incubated at room temperature for 20 h at low rpm in dark conditions. Thermal denaturation of the enzyme was carried out at 80^{o}C for 10 min, and pelleted at 15,000g for 30 min at room temperature. The supernatant was dried under vacuum centrifugation to collect solutes. The solutes/substrates were purified by ethanol for 6 h at -20 ^{o}C and the supernatant was dried under vacuum centrifugation. The obtained pellet/substrate was stored at -20 ^{o}C for later use. A standard curve of the obtained ester was generated using A_{366} for measurement using a spectrophotometer.

Enzyme kinetic assay of OsCCR14

The activity of OsCCR14 was measured according to the protocols described (Park *et al.*, 2017; Sattler *et al.*, 2017). To a final volume of 210 µL of each reaction mixture consisting of 100 mM sodium phosphate buffer, pH 6.2, 0.25 mM NADPH (Cat. # 144935, SRL Pvt. Ltd., India), thioester substrate (5 µM, 10 µM, 20 µM, 50 µM and 100 µM), 3 µg purified OsCCR14 was added and the enzyme reactions carried out at 30^{o}C. For reactions with OsCCR14 and OsATL53 complex, equal amounts of OsCCR14 and OsATL53 were first incubated at 4 ^{o}C for at least 2 h, quantified and 3 µg used per reaction. For reactions with JA, 100 µM JA was added to each reaction and incubated at 4 ^{o}C for 3 h. Reactions were initiated by the addition of the enzyme for 20 min with an interval of 1 min between reactions (20 reactions for one substrate concentration per reaction condition). Reactions were stopped by the addition of 40 µL of 15% (w/v) trichloroacetic acid and mixed well. These were then centrifuged briefly and 200 µL of each reaction mix was loaded onto a Corning clear 96-well plate. Decrease in A_{366} (substrate concentration) was recorded using a Tecan M200 microplate reader (Tecan Austria GmbH) and the i-control 1.7 software (Tecan Austria GmbH). K_m, V_{max} and K_{cat} values were determined by extrapolation from Lineweaver-Burk plots. Each enzyme assay was carried out for five times and the average values represented the mean ± standard deviation.

Declarations

Funding: The Department of Biotechnology, Government of India (BT/PR12394/AGIII/103/891/2014) provided the financial support. J.P.K. also acknowledges the award of J.C. Bose National Fellowship by the SERB, Government of India (SB/S2/JCB-13/2013); P.B. availed the Research Associateship sanctioned as part of the DBT project. A.S. would like to thank the University Grants Commission, New Delhi, for the award of a Research Fellowship. For infrastructural support, authors acknowledge the financial assistance provided by the Department of Science and Technology (through FIST and PURSE Grants), the University Grants Commission (through UGC-SAP grant) and the University of Delhi.

Acknowledgements: We are thankful to Ms. Charu Tanwar of CIF, University of Delhi South Campus, for her technical advice in the FLIM-FRET analyses.

Conflicts of interest/Competing interests: The authors declare no real or perceived interests.

Availability of data and materials: All data and materials will be available on request.

Code availability: N/A

Conflicts of Interest: The authors declare no real or perceived conflicts.

Author contributions: P.B. designed the experiments and wrote the paper. P.B. and A.S. carried out the experiments. J.P.K. supervised the work and critically edited the article.

References

Aguilar-Hernández V, Aguilar-Henonin L, Guzmán P (2011) 'Diversity in the architecture of ATLs, a family of plant ubiquitin-ligases, leads to recognition and targeting of substrates in different cellular environments'. PLoS One 6(8):e23934

Alam I, Yang YQ, Wang Y, Zhu ML, Wang HB, Chalhoub B, Lu YH (2017) 'Genome-wide identification, evolution and expression analysis of RING finger protein genes in Brassica rapa'. Sci Rep 7:40690

Anzilotti C, Swan DJ, Boisson B, Deobagkar-Lele M, Oliveira C, Chabosseau P, Engelhardt KR, Xu X, Chen R, Alvarez L, Berlinguer-Palmini R, Bull KR, Cawthorne E, Cribbs AP, Crockford TL, Dang TS, Fearn A, Fenech EJ, de Jong SJ, Lagerholm BC, Ma CS, Sims D, van den Berg B, Xu Y, Cant AJ, Kleiner G, Leahy TR, de la Morena MT, Puck JM, Shapiro RS, van der Burg M, Chapman JR, Christianson JC, Davies B, McGrath JA, Przyborski S, Koref S, Tangye M, Werner SG, Rutter A, Padilla-Parra GA, Casanova S, Cornall JL, Conley RJ, M. E. and Hambleton, S (2019) Nat Immunol 20(3):350–361 'An essential role for the Zn'

Borah P, Khurana JP (2018) 'The OsFBK1 E3 Ligase Subunit Affects Anther and Root Secondary Cell Wall Thickenings by Mediating Turnover of a Cinnamoyl-CoA Reductase'. Plant Physiol 176(3):2148–2165

Buetow L, Huang DT (2016) 'Structural insights into the catalysis and regulation of E3 ubiquitin ligases'. Nat Rev Mol Cell Biol 17(10):626–642

Cecchetti V, Altamura MM, Brunetti P, Petrocelli V, Falasca G, Ljung K, Costantino P, Cardarelli M (2013) 'Auxin controls Arabidopsis anther dehiscence by regulating endothecium lignification and jasmonic acid biosynthesis'. Plant J 74(3):411–422

Cecchetti V, Altamura MM, Falasca G, Costantino P, Cardarelli M (2008) 'Auxin regulates Arabidopsis anther dehiscence, pollen maturation, and filament elongation'. Plant Cell 20(7):1760–1774

D'Angiolella V, Donato V, Forrester FM, Jeong YT, Pellacani C, Kudo Y, Saraf A, Florens L, Washburn MP, Pagano M (2012) 'Cyclin F-mediated degradation of ribonucleotide reductase M2 controls genome integrity and DNA repair'. Cell 149(5):1023–1034

Deng XW, Matsui M, Wei N, Wagner D, Chu AM, Feldmann KA, Quail PH (1992) 'COP1, an Arabidopsis regulatory gene, encodes a protein with both a zinc-binding motif and a G beta homologous domain'. Cell 71(5):791–801

Devoto A, Nieto-Rostro M, Xie D, Ellis C, Harmston R, Patrick E, Davis J, Sherratt L, Coleman M, Turner JG (2002) 'COI1 links jasmonate signalling and fertility to the SCF ubiquitin-ligase complex in Arabidopsis'. Plant J 32(4):457–466

Disch S, Anastasiou E, Sharma VK, Laux T, Fletcher JC, Lenhard M (2006) 'The E3 ubiquitin ligase BIG BROTHER controls arabidopsis organ size in a dosage-dependent manner'. Curr Biol 16(3):272–279

Dong CH, Agarwal M, Zhang Y, Xie Q, Zhu JK (2006) 'The negative regulator of plant cold responses, HOS1, is a RING E3 ligase that mediates the ubiquitination and degradation of ICE1'. Proc Natl Acad Sci U S A 103(21):8281–8286

Freemont PS (2000) 'RING for destruction?'. Curr Biol 10(2):R84–R87

Freemont PS, Hanson IM, Trowsdale J (1991) 'A novel cysteine-rich sequence motif'. Cell 64(3):483–484

Furukawa M, Zhang Y, McCarville J, Ohta T, Xiong Y (2000) 'The CUL1 C-terminal sequence and ROC1 are required for efficient nuclear accumulation, NEDD8 modification, and ubiquitin ligase activity of CUL1'. Mol Cell Biol 20(21):8185–8197

Goldberg RB, Beals TP, Sanders PM (1993) 'Anther development: basic principles and practical applications'. Plant Cell 5(10):1217–1229

Greve K, La Cour T, Jensen MK, Poulsen FM, Skriver K (2003) 'Interactions between plant RING-H2 and plant-specific NAC (NAM/ATAF1/2/CUC2) proteins: RING-H2 molecular specificity and cellular localization'. Biochem J 371(Pt 1):97–108

Guzmán P (2012) 'The prolific ATL family of RING-H2 ubiquitin ligases'. Plant Signal Behav 7(8):1014–1021

Guzmán P (2014) 'ATLs and BTLs, plant-specific and general eukaryotic structurally-related E3 ubiquitin ligases', *Plant Sci*, 215–216, pp. 69–75

Hardtke CS, Okamoto H, Stoop-Myer C, Deng XW (2002) 'Biochemical evidence for ubiquitin ligase activity of the Arabidopsis COP1 interacting protein 8 (CIP8)'. Plant J 30(4):385–394

Hua Z, Vierstra RD (2011) 'The cullin-RING ubiquitin-protein ligases'. Annu Rev Plant Biol 62:299–334

Hua Z, Zou C, Shiu SH, Vierstra RD (2011) 'Phylogenetic comparison of F-Box (FBX) gene superfamily within the plant kingdom reveals divergent evolutionary histories indicative of genomic drift'. PLoS One 6(1):e16219

Ishiguro S, Kawai-Oda A, Ueda J, Nishida I, Okada K (2001) 'The DEFECTIVE IN ANTHER DEHISCIENCE gene encodes a novel phospholipase A1 catalyzing the initial step of jasmonic acid biosynthesis, which synchronizes pollen maturation, anther dehiscence, and flower opening in Arabidopsis'. Plant Cell 13(10):2191–2209

Jackson PK, Eldridge AG, Freed E, Furstenthal L, Hsu JY, Kaiser BK, Reimann JD (2000) 'The lore of the RINGs: substrate recognition and catalysis by ubiquitin ligases'. Trends Cell Biol 10(10):429–439

Jain M, Nijhawan A, Arora R, Agarwal P, Ray S, Sharma P, Kapoor S, Tyagi AK, Khurana JP (2007) 'F-box proteins in rice. Genome-wide analysis, classification, temporal and spatial gene expression during panicle and seed development, and regulation by light and abiotic stress'. Plant Physiol 143(4):1467–1483

Jiménez-López D, Aguilar-Henonin L, González-Prieto JM, Aguilar-Hernández V, Guzmán P (2018a) 'CTLs, a new class of RING-H2 ubiquitin ligases uncovered by YEELL, a motif close to the RING domain that is present across eukaryotes'. PLoS One 13(1):e0190969

Jiménez-López D, Muñóz-Belman F, González-Prieto JM, Aguilar-Hernández V, Guzmán P (2018b) 'Repertoire of plant RING E3 ubiquitin ligases revisited: New groups counting gene families and single genes'. PLoS One 13(8):e0203442

Kawasaki T, Koita H, Nakatsubo T, Hasegawa K, Wakabayashi K, Takahashi H, Umemura K, Umezawa T, Shimamoto K (2006) 'Cinnamoyl-CoA reductase, a key enzyme in lignin biosynthesis, is an effector of small GTPase Rac in defense signaling in rice'. Proc Natl Acad Sci U S A 103(1):230–235

Kelly CE, Thymiakou E, Dixon JE, Tanaka S, Godwin J, Episkopou V (2013) 'Rnf165/Ark2C enhances BMP-Smad signaling to mediate motor axon extension'. PLoS Biol 11(4):e1001538

Lambert TJ (2019) 'FPbase: a community-editable fluorescent protein database'. Nat Methods 16(4):277–278

Lim SD, Yim WC, Moon JC, Kim DS, Lee BM, Jang CS (2010) 'A gene family encoding RING finger proteins in rice: their expansion, expression diversity, and co-expressed genes'. Plant Mol Biol 72(4–5):369–380

Liu J, Zhang Y, Qin G, Tsuge T, Sakaguchi N, Luo G, Sun K, Shi D, Aki S, Zheng N, Aoyama T, Oka A, Yang W, Umeda M, Xie Q, Gu H, Qu LJ (2008) 'Targeted degradation of the cyclin-dependent kinase inhibitor ICK4/KRP6 by RING-type E3 ligases is essential for mitotic cell cycle progression during Arabidopsis gametogenesis'. Plant Cell 20(6):1538–1554

Nagels Durand A, Pauwels L, Goossens A (2016) 'The Ubiquitin System and Jasmonate Signaling', *Plants (Basel)*, 5(1)

Noureddine MA, Donaldson TD, Thacker SA, Duronio RJ (2002) 'Drosophila Roc1a encodes a RING-H2 protein with a unique function in processing the Hh signal transducer Ci by the SCF E3 ubiquitin ligase'. Dev Cell 2(6):757–770

Park HL, Bhoo SH, Kwon M, Lee SW, Cho MH (2017) 'Biochemical and Expression Analyses of the Rice Cinnamoyl-CoA Reductase Gene Family', *Front Plant Sci*, 8, pp. 2099

Peng YJ, Shih CF, Yang JY, Tan CM, Hsu WH, Huang YP, Liao PC, Yang CH (2013) 'A RING-type E3 ligase controls anther dehiscence by activating the jasmonate biosynthetic pathway gene DEFECTIVE IN ANTHER DEHISCENCE1 in Arabidopsis'. Plant J 74(2):310–327

Poulsen SL, Hansen RK, Wagner SA, van Cuijk L, van Belle GJ, Streicher W, Wikström M, Choudhary C, Houtsmuller AB, Marteijn JA, Bekker-Jensen S, Mailand N (2013) 'RNF111/Arkadia is a SUMO-targeted ubiquitin ligase that facilitates the DNA damage response'. J Cell Biol 201(6):797–807

Salinas-Mondragón RE, Garcidueñas-Piña C, Guzmán P (1999) 'Early elicitor induction in members of a novel multigene family coding for highly related RING-H2 proteins in Arabidopsis thaliana'. Plant Mol Biol 40(4):579–590

Sanders PM, Lee PY, Biesgen C, Boone JD, Beals TP, Weiler EW, Goldberg RB (2000) 'The arabidopsis DELAYED DEHISCENCE1 gene encodes an enzyme in the jasmonic acid synthesis pathway'. Plant Cell 12(7):1041–1061

Sattler SA, Walker AM, Vermerris W, Sattler SE, Kang C (2017) 'Structural and Biochemical Characterization of Cinnamoyl-CoA Reductases'. Plant Physiol 173(2):1031–1044

Serrano M, Guzmán P (2004) 'Isolation and gene expression analysis of Arabidopsis thaliana mutants with constitutive expression of ATL2, an early elicitor-response RING-H2 zinc-finger gene'. Genetics 167(2):919–929

Serrano M, Parra S, Alcaraz LD, Guzmán P (2006) 'The ATL gene family from Arabidopsis thaliana and Oryza sativa comprises a large number of putative ubiquitin ligases of the RING-H2 type'. J Mol Evol 62(4):434–445

Sheard LB, Tan X, Mao H, Withers J, Ben-Nissan G, Hinds TR, Kobayashi Y, Hsu FF, Sharon M, Browse J, He SY, Rizo J, Howe GA, Zheng N (2010) 'Jasmonate perception by inositol-phosphate-potentiated COI1-JAZ co-receptor'. Nature 468(7322):400–405

Sheren JE, Kassenbrock CK (2013) 'RNF38 encodes a nuclear ubiquitin protein ligase that modifies p53'. Biochem Biophys Res Commun 440(4):473–478

Sonoda Y, Yao SG, Sako K, Sato T, Kato W, Ohto MA, Ichikawa T, Matsui M, Yamaguchi J, Ikeda A (2007) 'SHA1, a novel RING finger protein, functions in shoot apical meristem maintenance in Arabidopsis'. Plant J 50(4):586–596

Stintzi A, Browse J (2000) 'The Arabidopsis male-sterile mutant, opr3, lacks the 12-oxophytodienoic acid reductase required for jasmonate synthesis'. Proc Natl Acad Sci U S A 97(19):10625–10630

Stone SL, Anderson EM, Mullen RT, Goring DR (2003) 'ARC1 is an E3 ubiquitin ligase and promotes the ubiquitination of proteins during the rejection of self-incompatible Brassica pollen'. Plant Cell 15(4):885–898

Trautmann S, Buschmann V, Orthaus S, Koberling F, Ortmann U, Erdmann R (2013) *Fluorescence lifetime imaging (FLIM) in confocal microscopy applications: an overview*

Vierstra RD (2009) 'The ubiquitin-26S proteasome system at the nexus of plant biology'. Nat Rev Mol Cell Biol 10(6):385–397

Xie DX, Feys BF, James S, Nieto-Rostro M, Turner JG (1998) 'COI1: an Arabidopsis gene required for jasmonate-regulated defense and fertility'. Science 280(5366):1091–1094

Xie Q, Guo HS, Dallman G, Fang S, Weissman AM, Chua NH (2002) 'SINAT5 promotes ubiquitin-related degradation of NAC1 to attenuate auxin signals'. Nature 419(6903):167–170

Xu R, Li QQ (2003) 'A RING-H2 zinc-finger protein gene RIE1 is essential for seed development in Arabidopsis'. Plant Mol Biol 53(1–2):37–50

Zhang X, Garreton V, Chua NH (2005) 'The AIP2 E3 ligase acts as a novel negative regulator of ABA signaling by promoting ABI3 degradation'. Genes Dev 19(13):1532–1543

Figures

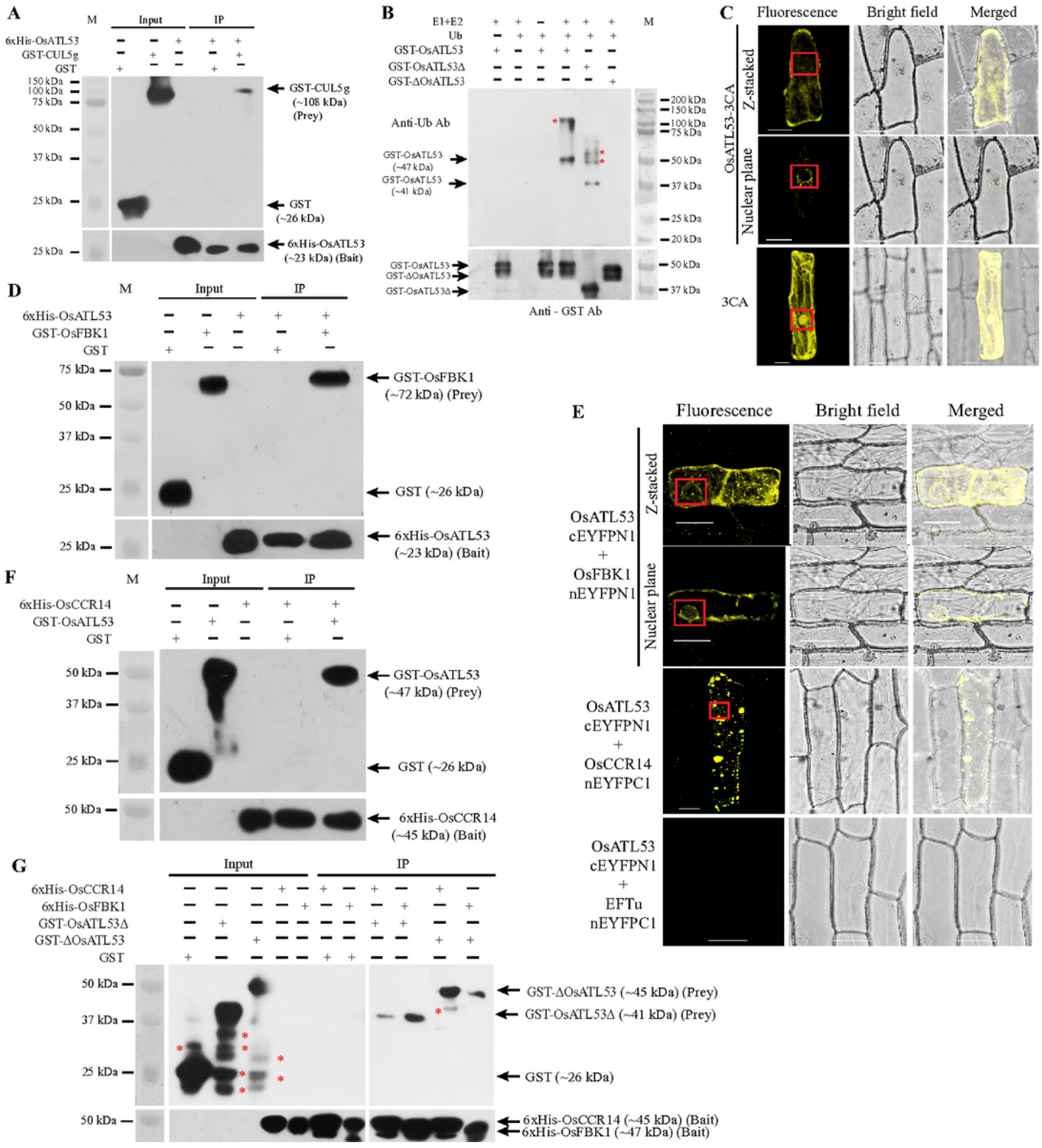

Figure 1

Interaction studies of OsATL53. A. In vitro immunoprecipitation assay between GST-CUL5g and 6xHis-OsATL53. Lanes 2, 3 and 4 are the unpurified input bacterial extracts of GST, GST-CUL5g and 6xHis-OsATL53, respectively. GST wash was used as a negative control for IP with 6xHis-OsFBK1 (lane 5). GST-tagged proteins were probed by rabbit anti-GST mAb, while 6xHis-OsATL53 was detected by using mouse anti-His mAb. These blots were parallelly processed with the same samples. M - Marker lane with the

designated protein bands. B. In vitro auto-ubiquitintion assay to determine E3 property of OsATL53. Controls used are GST-OsATL53Δ and GST-ΔOsATL53 respectively. Arrows determine the positions of ubiquitinated OsATL53/GST-OsATL53Δ in top panel, red asterisks indicate non-specific bands. Bottom panel shows the input proteins as probed by anti-GST mAb. C. Representative image of cellular localization of OsATL53 in onion epidermal peel cells. Control: pSITE-3CA vector. Bright field images show the location of the nuclei in all panels. Bar- 50 μm. Red boxes denote nucleus. D. In vitro immunoprecipitation assay between GST-OsFBK1 and 6xHis-OsATL53. GST wash (lane 2) was used as the negative control. Lanes 3 and 4 show the input bacterial extracts of GST-OsFBK1 and 6xHis-OsATL53 respectively. Lanes 5 and 6 are the IP lanes. E. YFP fluorescence showing the BiFC between OsATL53/OsFBK1 (upper panel) and OsATL53/OsCCR14 (middle panel) respectively in a representative cell. Bright field images show the location of the nuclei. Negative control: BiFC between OsATL53 and EFTu (lower panel). Bar- 50 μm. Red boxes denote nucleus. F. IP between GST-OsATL53 and 6xHis-OsCCR14. G. Western blot showing the IPs between GST-ΔOsATL53/ GST-OsATL53Δ and OsCCR14 and OsFBK1 respectively. Red asterisks denote non-specifc binding. For all IPs, GST and GST-tagged proteins were probed by rabbit anti-GST mAb, His-tagged proteins were detected by mouse anti-His mAb. M-marker lane for both blots. See also Fig. S1.

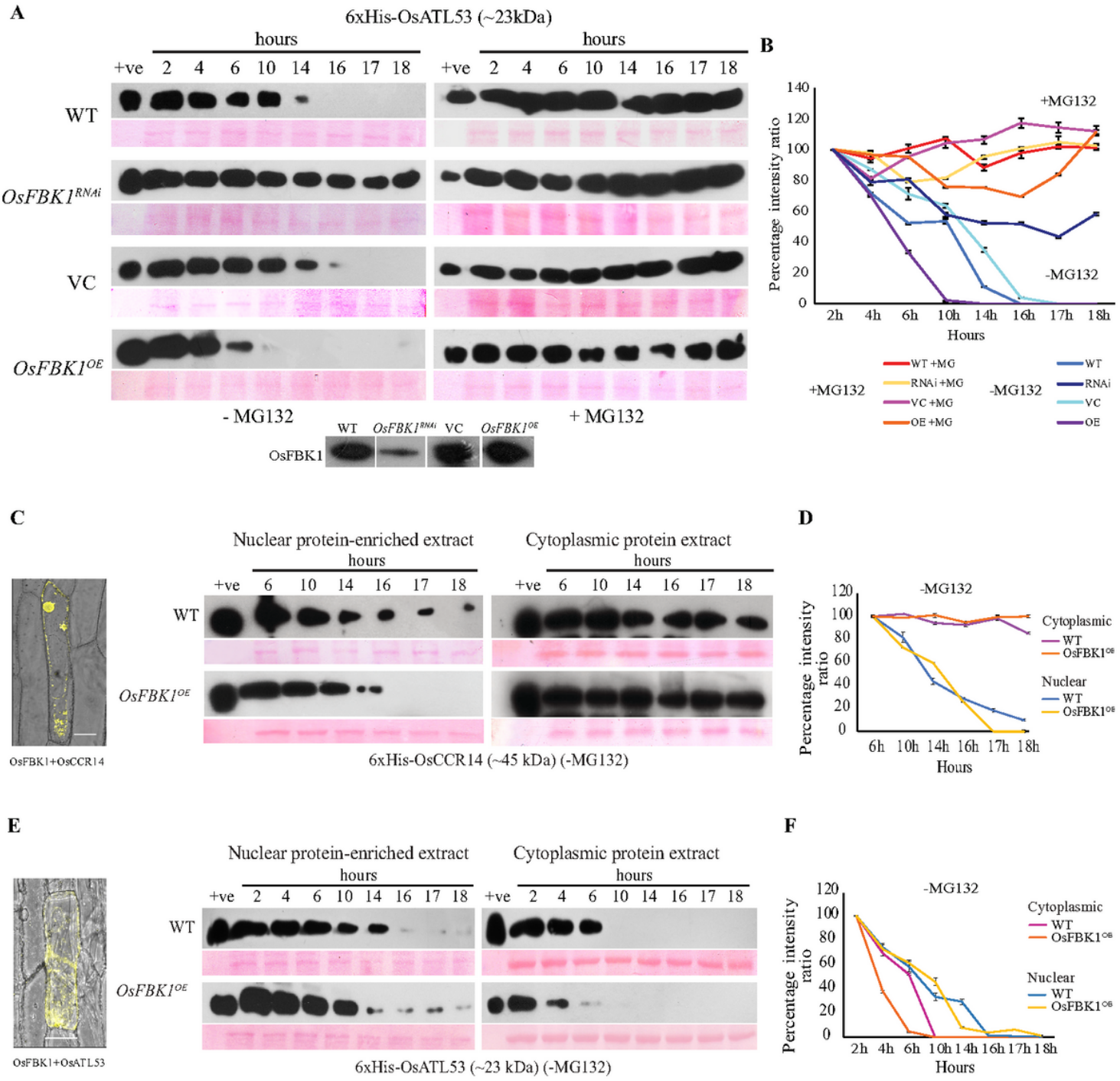

Figure 2

Cell-free degradation of OsATL53 in plant protein extracts. A. Time-scale degradation assay of 5 µg 6xHis-OsATL53 in 30 µg cell-free whole seedling protein extracts of control and OsFBK1 transgenics both with and without MG132. Loading control depicted by the Ponceau stained Rubisco large subunit band (55 kDa) for all. The bottom-most panel shows the level of OsFBK1 in the plant materials used, as probed by anti-OsFBK1 antibodies described earlier (Borah and Khurana, 2018). B. Graphical representation of degradation kinetics data of OsATL53. Error bars denote SD. C. Degradation assay of 6xHis-OsCCR14 in

the nuclear protein-enriched and cytoplasmic protein extracts of WT and OsFBK1OE seedlings without MG132. The time points used were as described before (Borah and Khurana, 2018). The confocal image on the left shows the BiFC interaction between OsFBK1 and OsCCR14 in onion peel cells. Loading controls are Ponceau stained Rubisco (55 kDa) for cytoplasmic extracts and histone H3 band (15 kDa) for nuclear protein-enriched extracts respectively. D. Graphical representation of the same where error bars denote SD. E. Cell-free degradation time kinetics of 6xHis-OsATL53 in the nuclear protein-enriched and cytoplasmic protein extracts of WT and OsFBK1OE seedlings without MG132. Image of BiFC between OsFBK1 and OsATL53 in onion epidermal peel cells is shown on the left. Loading controls, histone H3 and Rubisco large subunit as mentioned above. F. Percentage intensity ratio graph of OsATL53 degradation in the cell-free systems. Error bars denote SD.

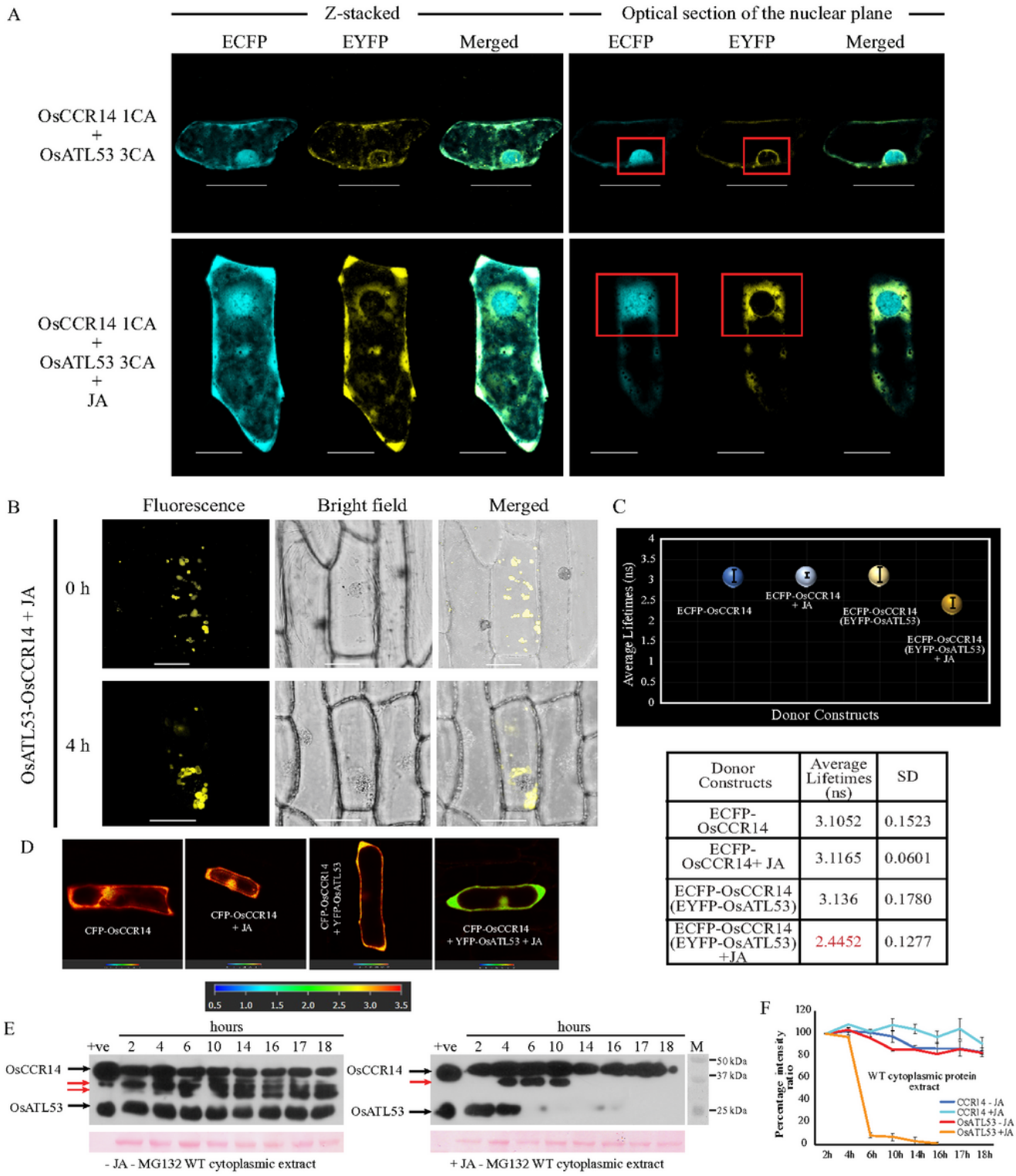

Donor Constructs	Average Lifetimes (ns)	SD
ECFP-OsCCR14	3.1052	0.1523
ECFP-OsCCR14+ JA	3.1165	0.0601
ECFP-OsCCR14 (EYFP-OsATL53)	3.136	0.1780
ECFP-OsCCR14 (EYFP-OsATL53) +JA	2.4452	0.1277

Figure 3

Jasmonic acid induced changes in sub-cellular location and conformation of OsATL53-OsCCR14 complex. A. Co-localization of OsCCR14-ECFP and OsATL53-EYFP in onion peel cells. Upper panel shows ECFP and EYFP fluorescence without JA treatment, while lower panel shows changes in EYFP fluorescence after 4 hours of JA treatment. Red boxes show the accumulation of ECFP and EYFP fluorescence around the target cell's nucleus before and after JA treatment. B. Movement of OsATL53-

OsCCR14 BiFC complex in response to 6.4mM JA observed after 4 hours. Bright field images show the location of the nucleus in the representative target cell. Bar- 50 µm. C. Change in lifetime of ECFP-OsCCR14 donor construct upon exposure to JA under FLIM-FRET conditions. Error bars denote SD of at least 5 cells observed. D. Representative Fast FLIM images of target cells in normal and JA-induced conditions. Positive FRET is present through-out the cell. Bar represents the range of lifetimes from 0.5-3.5 ns. E. Cell-free degradation of 6xHis-OsCCR14 and 6xHis-OsATL53 in the cytoplasmic protein extracts of WT seedlings, in the absence and presence of JA respectively. Time kinetics performed in the absence of MG132. Loading control: Ponceau stained Rubisco large subunit band (55 kDa). Red arrows denote non-specific binding. M - marker lane. F. Graphical representation of cell-free degradation kinetics where error bars denote SD. See Fig. S3-S6.

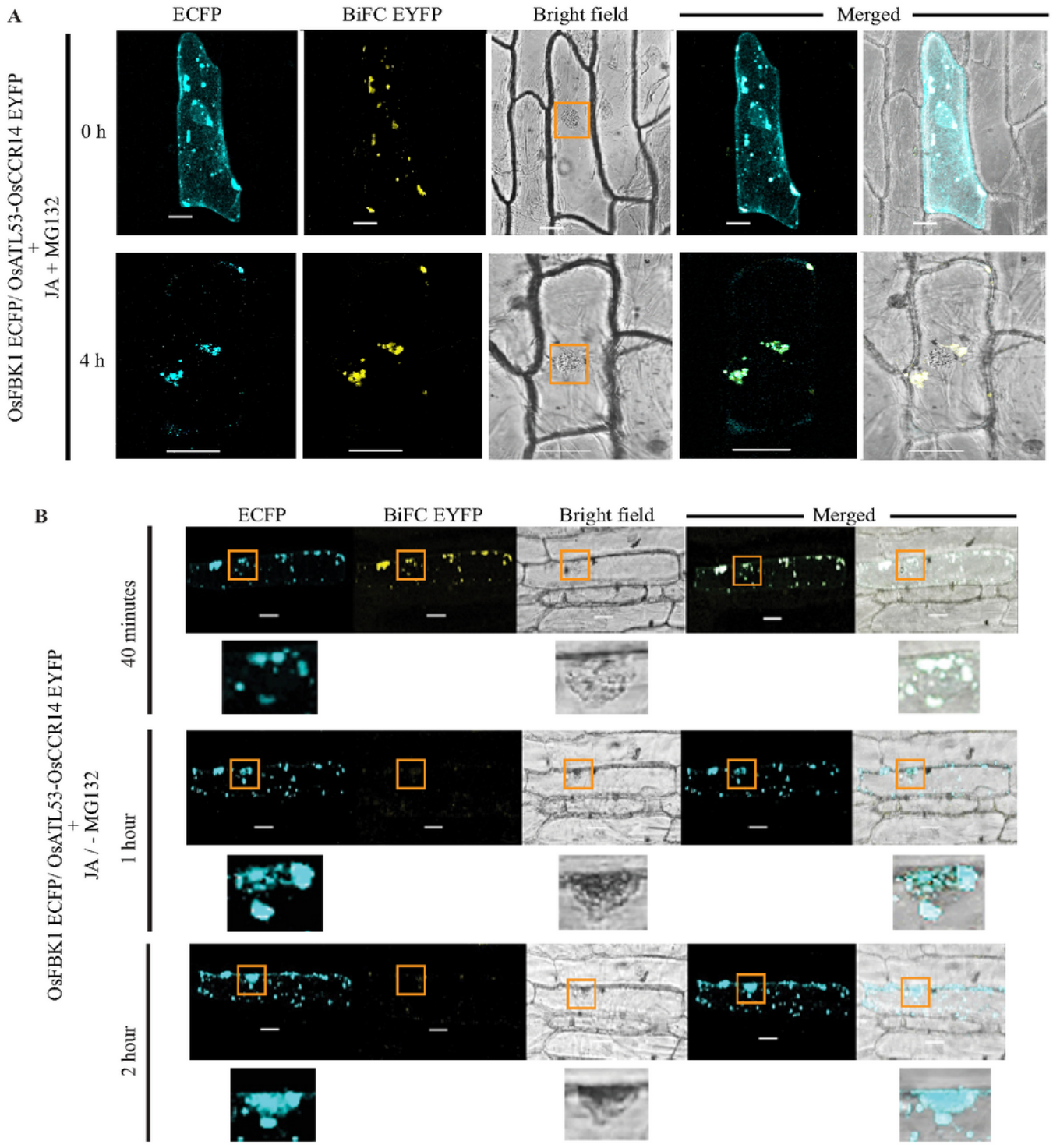

Figure 4

Changes in protein interaction and localization dynamics in the presence of JA. A. OsFBK1 ECFP fluorescence was observed to merge with the BiFC (OsATL53-OsCCR14) EYFP fluorescence (Z-stacked) after 2 hours of JA exposure and accumulate around the nuclear boundary after 4 hours, in the presence of MG132. B. Changes in localization pattern of OsFBK1 after JA without MG132 treatment in presence of OsCCR14-OsATL53 complex. After degradation of OsATL53 and the disruption of the OsCCR14-

OsATL53 complex and loss of EYFP signal, the normal localization pattern of OsFBK1 is seen. The same target cell was observed after the requisite time points after JA treatment. A loss in signal strength was observed due to repeated laser exposure, and the ECFP and EYFP fluorescence were adjusted accordingly. The orange boxes and inset pictures below each panel focusses the nucleus. Bright field images show the location of the nucleus in each target cell. Merged pictures are shown in both dark and bright field background. Green colour denotes overlapped regions of ECFP and EYFP fluorescence. Bar - 50 µm. See Fig. S7.

A

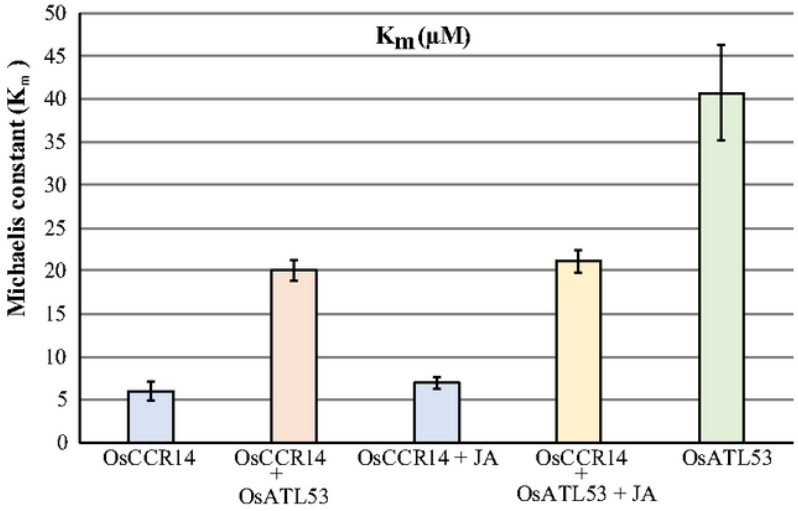

B

Sample	K_m (µM)	K_{cat} (s^{-1})	K_{cat}/K_m ($s^{-1}µM^{-1}$)
OsCCR14	6.006 ± 1.1075	3.8978e -4 ± 0.0029	6.41e -5 ± 4.45e-5
OsCCR14 + OsATL53	20.0461 ± 1.2642	3.5456e -4 ± 6.27e-5	2.1234e -5 ± 1.39e-5
OsCCR14 + JA	6.9571 ± 0.7292	2.28e-4 ± 1. 68e-5	3.3124e -5 ± 4.28e-6
OsCCR14 + OsATL53 + JA	21.0866 ± 1.2854	2.8972e -4 ± 1.79e-4	1.4256e-5 ± 9.12e-6
OsATL53	40.7378 ± 5.5711	3.3370e-4 ± 4.96e-5	1.0132e-5 ±2.49e - 6

Figure 5

Kinetic parameters of the enzymatic activities of OsCCR14 under different conditions. A: Graphical representation of the Km values of OsCCR14 either alone or in a complex with OsATL53, with or without JA. B: Tabular representation of the observed kinetic parameters of the various enzyme combinations.

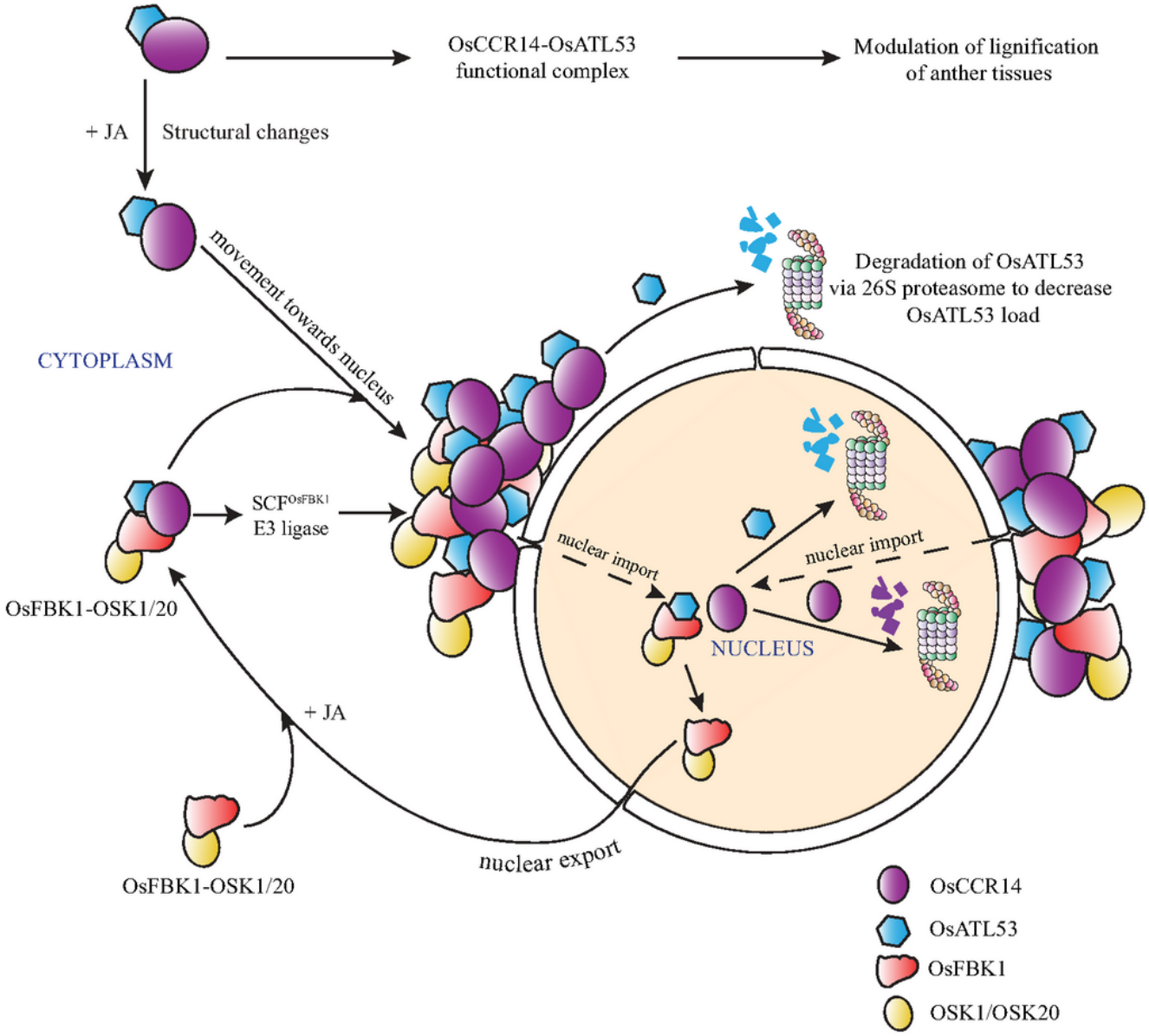

Figure 6

Proposed model of the signalling pathway involved in the jasmonic acid-mediated degradation of OsATL53 and OsCCR14 by SCFOsFBK1 and the 26S proteasome. OsFBK1 interacting with OSK1/OSK20 has been reported earlier (Borah and Khurana, 2018). See text for more details.

Supplementary Files

This is a list of supplementary files associated with this preprint. Click to download.

- SupplementaryInformationPMB.pdf